PERGAMON

Journal of Structural Geology 21 (1999) 729–742

JOURNAL OF STRUCTURAL GEOLOGY

Geometrical analysis of folded surfaces using simple functions[1]

F. Bastida[a,*], J. Aller[a], N.C. Bobillo-Ares[b]

[a]Departamento de Geología, Universidad de Oviedo, 33005 Oviedo, Spain
[b]Departamento de Matemáticas, Universidad de Oviedo, 33005 Oviedo, Spain

Received 4 August 1998; accepted 26 March 1999

Abstract

Several functions have been chosen in order to approximate fold profile geometry. Some of them are valid mainly for alloclinal folds (interlimb angle > 0), whereas others are mainly valid for isoclinal folds (interlimb angle = 0). In all cases, a fold profile can be characterised by an aspect ratio (y_0/x_0) between the height and the width of a limb (fold amplitude), and a shape parameter characteristic of the considered function. The shape parameters have been mutually linked through the area beneath the fold profile. The geometrical analysis enables a graphical classification based on a shape–amplitude diagram in which the most common types of folded surfaces are represented: cuspate, chevron, sinusoidal, parabolic, elliptic and box folds. Any of the shape parameters can be used as x-axis of the diagram in order to approximate the geometries commonly exhibited by natural folds. In the diagram presented in this paper two shape parameters have been combined: the exponent n of a power function for alloclinal folds, and a parameter C/y_0, defined from a function composed of an elliptic part and a line segment of length C for isoclinal folds. In order to show the suitability of the classification method, it has been applied to some examples of finite-element, experimental and natural folds.

1. Introduction

The determination of the strain distribution in folded layers is seldom possible at present. As a consequence, the precise knowledge of the geometry of folds is in many cases the only tool available to analyse the origin and evolution of these structures. To systematise the fold geometry depends on the availability of adequate methods for the geometrical description of folds. To date this description has focused on two aspects: the geometry of single folded surfaces and the geometry of folded layers.

The fold classification proposed by Ramsay (1967, pp. 359–372) is a powerful tool to analyse in detail the profile geometry of folded layers. Some problems of this classification were analysed by Hudleston (1973) and complementary methods to classify large data sets of folds were developed by Bastida (1993) and Lisle (1997).

Several parameters have been used to characterise the morphology of single folded surfaces. A classical parameter to describe the fold tightness is the interlimb angle (ϕ), which was used by Fleuty (1964) to differentiate the following types of folds: gentle ($180 > \phi > 120^\circ$), open ($120 \geq \phi > 70^\circ$), close ($70 \geq \phi > 30^\circ$), tight ($30 \geq \phi > 0^\circ$), isoclinal ($\phi = 0^\circ$), and elasticas ($\phi < 0^\circ$). Because the shape of the folded surface in cross-section also depends on the changes in curvature, Ramsay (1967) defined two parameters: P_1, which is the extent of the fold limbs with respect to that of the hinge zone; and P_2, which is obtained by expressing the maximum curvature of the fold surface as a ratio of the unit curvature of the circle drawn with the distance between the inflection points as a diameter.

Another approach to the geometrical analysis of the folded surfaces in cross-section is based on Fourier analysis, each limb being characterised by several coefficients of a Fourier sine series (Stabler, 1968; Hudleston, 1973; Ramsay and Huber, 1987,

* Corresponding author.
E-mail address: bastida@asturias.geol.uniovi.es (F. Bastida)

[1] Information and software on the fold classification developed in this paper are available in: http://www.geol.uniovi.es/folds.html

0191-8141/99/$ - see front matter
PII: S0191-8141(99)00079-6

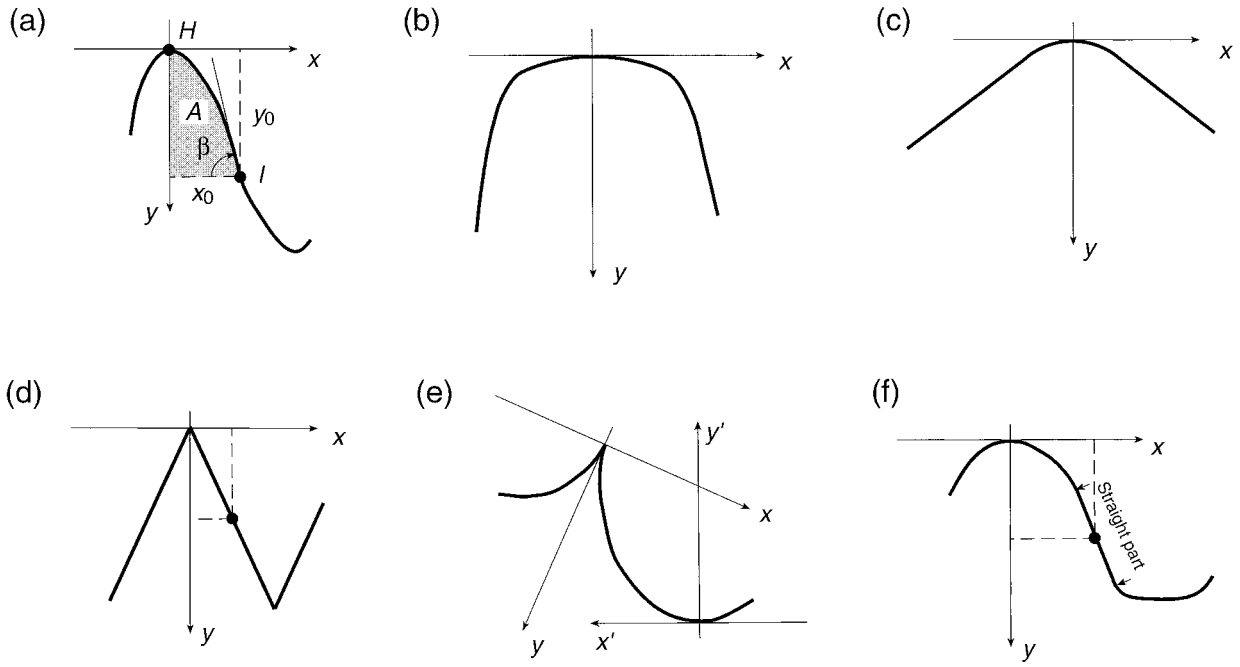

Fig. 1. Reference system and geometrical elements used in this study. (a) General case: H, hinge point; I, inflection point; A, area beneath the limb profile; β, maximum dip. (b) Double hinge fold. (c) Fold with a circular arc. (d) Chevron fold. (e) Cuspate fold. (f) Fold with a straight segment in the limb.

pp. 314–316; Stowe, 1988). The advantage of this method is that a limb is approximated by a mathematical function; nevertheless, this function is very complicated, particularly when a large number of coefficients are involved (Stowe, 1988). In addition, the use of many coefficients is inconvenient for classification purposes. Hudleston (1973) used two Fourier coefficients (b_1 and b_3) to classify the profile shape of folded surfaces through a graphical representation of b_1 vs b_3. Thus, this author distinguished six types of standard shapes, from type A (box folds) to F (chevron folds), and five standard amplitudes (1–5). A quick alternative to the measurements and calculations involved in this method of classification is the visual harmonic analysis (Hudleston, 1973), that allows the determination of b_1 and b_3 by comparing the fold profile with 30 idealised fold forms with different shapes (A–F) and amplitudes (1–5). Unfortunately, the use of two Fourier coefficients gives only a rough approximation to the functions that describe fold morphologies (Stowe, 1988).

Twiss (1988) proposed a classification of symmetric folded surfaces based on the determination of three fold style parameters. A problem of this classification is that the results of its application cannot be fully represented in two-dimensional diagrams. Moreover, the classification of asymmetric folds requires six parameters, and this makes its use difficult. On the other hand, this classification does not provide an analytical expression of the folded surface profile.

The aim of this paper is to present a geometrical analysis of folded surface profiles based on their approximation by simple functions, and plot the results on a graph which reflects and discriminates accurately the main geometrical features of the profiles and permits their classification.

2. Basis of the analysis

The geometrical analysis of a folded surface profile requires the selection of a reference system. The chosen system is formed by the tangent to the profile curve at the hinge point (x-axis) and its normal through this point (y-axis) (Fig. 1a). In the case of folds with a double hinge, the point equidistant from both hinges (closure point of Twiss, 1988) is chosen as co-ordinate origin (Fig. 1b), whereas in the case of a fold with an arc of constant curvature and without a defined hinge point, the middle point of this arc is considered as origin (Fig. 1c). In chevron and cuspate folds the y-axis is the bisector line of the interlimb or cusp angle, and the x-axis is perpendicular to the y-axis through the vertex or cusp point, respectively (Fig. 1d and e).

The unit considered for the analysis of folded surfaces is the fold limb profile, defined as the portion of the profile between the co-ordinate origin and an adjacent inflection point (Fig. 1a) (quarter wavelength unit of Hudleston, 1973). This definition is problematic in those folds in which the inflection point is not defined, such as (1) folds with a line segment in the limb, (2)

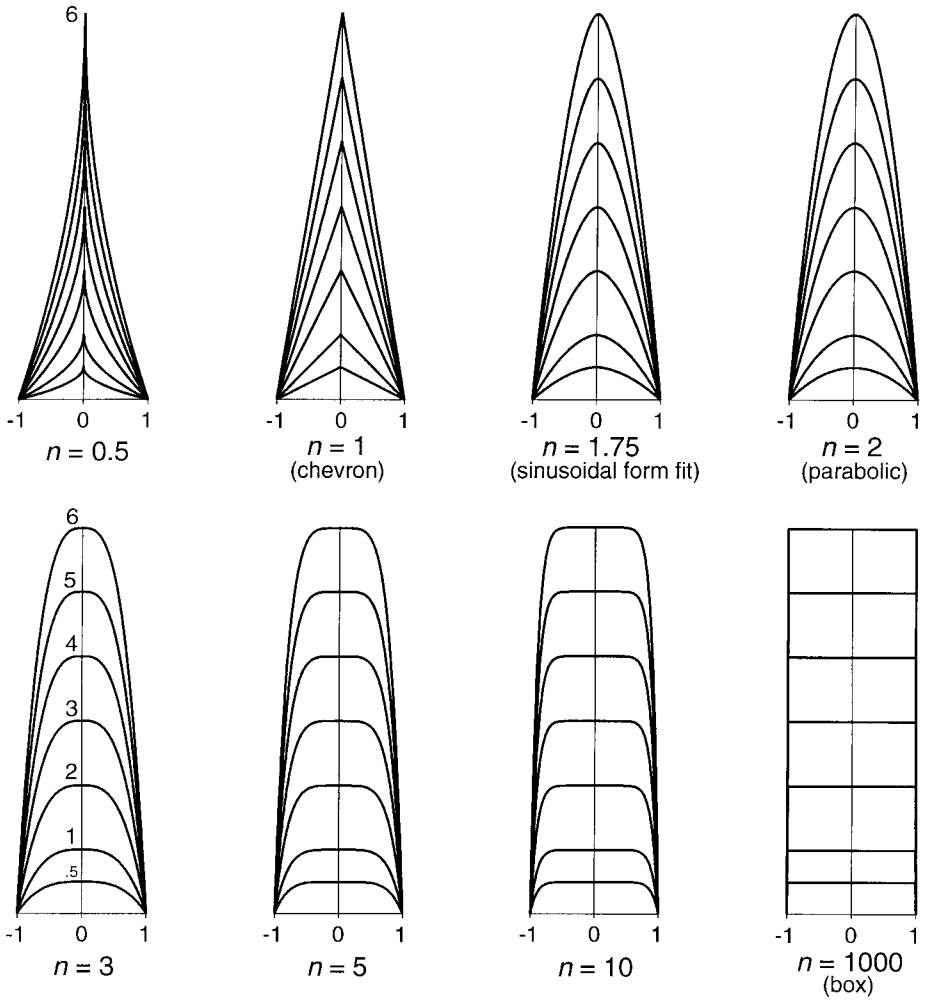

Fig. 2. Fold morphology corresponding to power functions with different values of y_0/x_0 and the exponent n. For a better visualisation of the folded profiles the origin of co-ordinates has been located in the fold core.

chevron folds, and (3) lobe-and-cusp folds. In cases (1) and (2), the limit between adjacent folds is taken in the middle point of the straight sector (Fig. 1d and f). In case (3), the arc between the cusp point and an adjacent hinge is taken as a limb that is common for the cuspate fold and the adjacent arc fold. Hence, in this case a single limb may be analysed twice with different reference axes, one for each type of fold (Fig. 1e).

Since it is difficult to find a single simple function which approximates adequately all the common fold morphologies found in rocks, it is convenient to separate folds into two categories: alloclinal folds (interlimb angle $> 0^\circ$) and isoclinal folds (interlimb angle $= 0^\circ$). Folds with interlimb angle $< 0^\circ$ are uncommon in deformed rocks and they are not analysed in this study.

2.1. Alloclinal folds

The geometry of a limb of an alloclinal folded surface profile may be approximated by several types of functions. The simplest is the power function given by:

$$\frac{y}{y_0} = \left(\frac{x}{x_0}\right)^n \tag{1}$$

defined within the interval $[0,x_0]$; n, x_0 and y_0 are positive numbers. The meaning of x_0 and y_0 is shown in Fig. 1(a), and x_0 is introduced in Eq. (1) to avoid the effect of the scale factor in the classification. In order to represent graphically a complete fold (the two adjacent limbs of an antiform or synform), Eq. (1) has been modified to:

$$\frac{y}{y_0} = \left(\frac{|x|}{x_0}\right)^n \tag{2}$$

considered within the interval $[-x_0,x_0]$. The ratio y_0/x_0 characterises the fold amplitude, whereas n characterises the fold shape. Fig. 2 illustrates the fold morphologies obtained for several values of n and y_0/x_0.

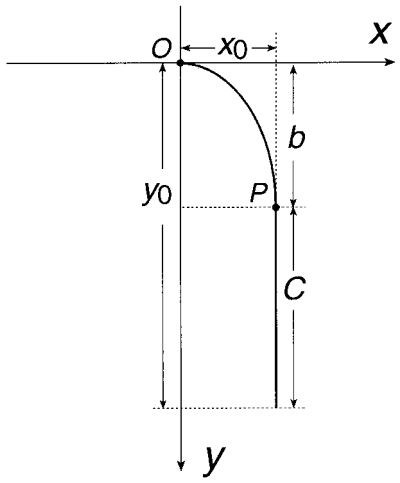

Fig. 3. Geometrical elements of an isoclinal fold.

The following values of n characterise some distinctive fold shapes: (1) $n<1$, cuspate folds; (2) $n=1$, chevron folds; (3) $n=2/(\pi-2)\approx 1.75$, fit of the sinusoidal folds; (4) $n=2$, parabolic folds; (5) $n>2$, double hinge folds (for n values close to 2, this morphology is visually imperceptible); (6) $n\rightarrow\infty$, box folds.

Another simple function that approximates the geometry of a limb of a folded surface profile is given by

$$y = y_0\left[1-\cos\left(\frac{\pi}{2}\frac{x}{x_0}\right)\right]^m \tag{3}$$

within the interval $[0,\pi/2]$. The meaning of x_0 and y_0 is indicated in Fig. 1(a), and m is a positive number. In this case, for $m<0.56$, we have cuspate folds; for $m\approx 0.56$, chevron folds; for $m=1$ sinusoidal folds; for $m>1$, double hinge folds (visually imperceptible for m values close to 1); and for $m\rightarrow\infty$, box folds. This function can be helpful in some cases, but it is more complicated than Eq. (1).

2.2. Isoclinal folds

The power functions do not generate proper isoclinal forms (except when $n\rightarrow\infty$) and isoclinal rounded folds (e.g. semicircular or semi-elliptical folds) are only roughly approximated by these functions. Hence, another type of function must be considered to fit isoclinal folds. A limb profile of these folds can be approximated by the expressions:

$$y = b\left(1-\sqrt{1-\frac{x^2}{x_0^2}}\right) \text{ within } [0,x_0] \tag{4a}$$

$$x = x_0 \text{ within } b\le y\le y_0 \tag{4b}$$

where $y_0 = b + C$ (Fig. 3).

Eq. (4a) is a quarter of an ellipse with semi-axes x_0 (on the x-axis) and b (on the y-axis), and centred at the point $(0,b)$; Eq. (4b) represents a line segment of length C which is a prolongation of the ellipse arc (Fig. 3). Fig. 4 shows some isoclinal fold morphologies described by Eqs. (4a) and (4b) (within the interval $[-x_0,x_0]$ to represent complete folds), for $x_0=1$ and several values of C/y_0 and y_0. For $y_0=b$ (or $C/y_0=0$)

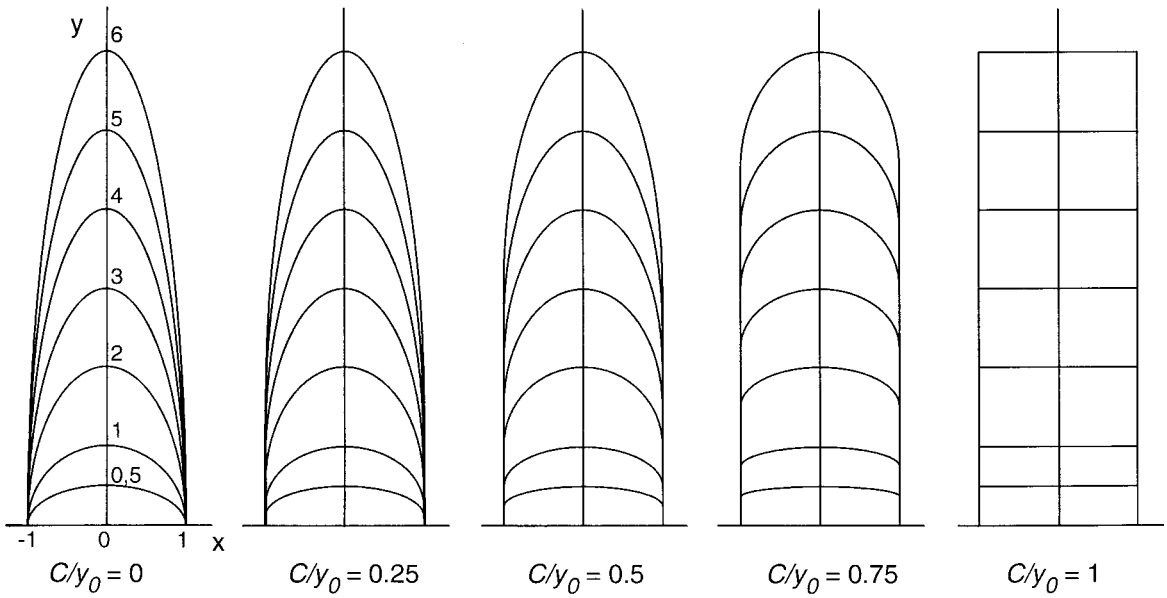

Fig. 4. Fold morphologies corresponding to Eqs. (4a) and (4b) for different values of y_0/x_0 and C. For a better visualisation of the folded profiles the origin of co-ordinates has been located in the fold core.

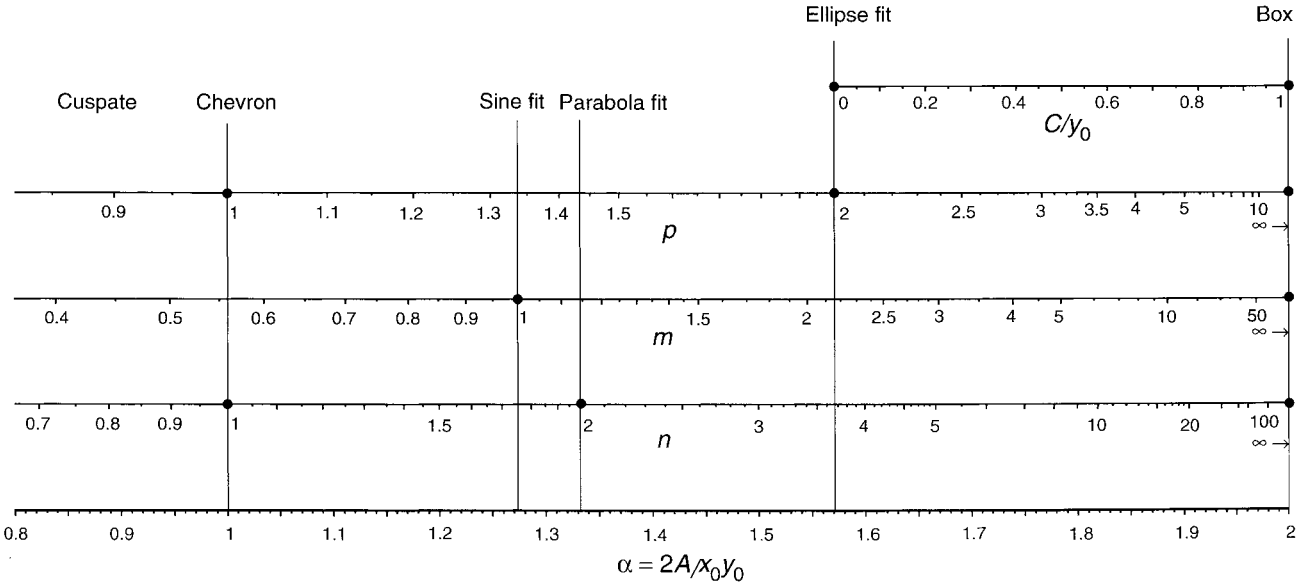

Fig. 5. Correlation scales for the shape parameters n, m, C/y_0 and p involved in Eqs. (1), (3), (4a), (4b) and (5), respectively. The basis for the correlation is the normalised area ($\alpha = 2A/x_0y_0$). Values of the shape parameters corresponding to chevron, and sine, parabola and ellipse fits have been correlated by vertical lines; the points on them indicate the perfect fit of the corresponding shapes.

folds are elliptical; for $x_0<b$ (or $C/y_0<1-x_0/y_0$) folds have a single hinge point; for $x_0 = b$, folds contain a semi-circle; for $x_0 > b$, the shape is that of double hinge folds; for $b = 0$ (or $C/y_0 = 1$), the shape is that of box folds.

Another function that can be used to analyse fold geometry is

$$\frac{x^p}{x_0^p} + \frac{y^p}{y_0^p} = 1. \tag{5}$$

This function was used by Lisle (1988) to approximate the form of coarse clastic sediment particles. For $p = 2$, this function describes an ellipse, whereas for $p<2$, it defines a family of curves named subellipses, and for $p > 2$, it represents curves named superellipses (Lisle, 1988, fig. 1). This function is suitable for both alloclinal ($p<2$) and isoclinal folds ($p\geq 2$). The maximum of Eq. (5) corresponds to the point $(0,y_0)$, and for $p<1$, we have cuspate folds; for $p = 1$, chevron folds; for $p = 2$, elliptic folds; and for $p\rightarrow\infty$, box folds. Eq. (5) fits fold shape better than Eqs. (1) and (3) or Eqs. (4a) and (4b) in some cases; nevertheless, it is more difficult to handle for analytical purposes than Eqs. (1), (4a) and (4b).

3. Fitting fold profiles to the theoretical functions

Once the functions that can be used to describe the fold profile geometry have been defined, it is necessary to establish fitting methods to approximate a natural fold by Eqs. (1), (3), (4a) and (4b) and/or Eq. (5). In some cases, the measurements necessary to fit a natural fold to one of the functions can be taken in the field; however, it is convenient to utilise photographs of the fold profile made with the optical axis of the camera perpendicular to the profile plane. The profile line of each limb and the corresponding reference frame can be drawn after these photographs, and x_0 and y_0 can be measured. In the case of isoclinal folds, the C value can also be measured directly, but the measurements commonly involve a large error. For this reason the parameter C should be always obtained using a best-fit method.

Two methods will be described to fit the profile line to one of the proposed functions: the fitting method by area balance, and the fitting method using the middle point. Since the y_0/x_0 value is a characteristic parameter of folds, in both methods we must search for a best-fit curve with the same y_0/x_0 value as the natural fold profile curve.

3.1. Fitting method by area balance

Balancing the area beneath the curves is an accurate technique to approximate the profile of a natural fold to any of the proposed functions. This fitting method requires the determination of the area A beneath the profile curve of a particular natural fold (see Fig. 1a). This determination can be made by a rule of numerical integration, by cutting-out the area within the fold profile and weighing it in a chemical balance (Cooper et al., 1983), or by a computer program which permits area estimation (e.g. CANVAS™). The next step is to

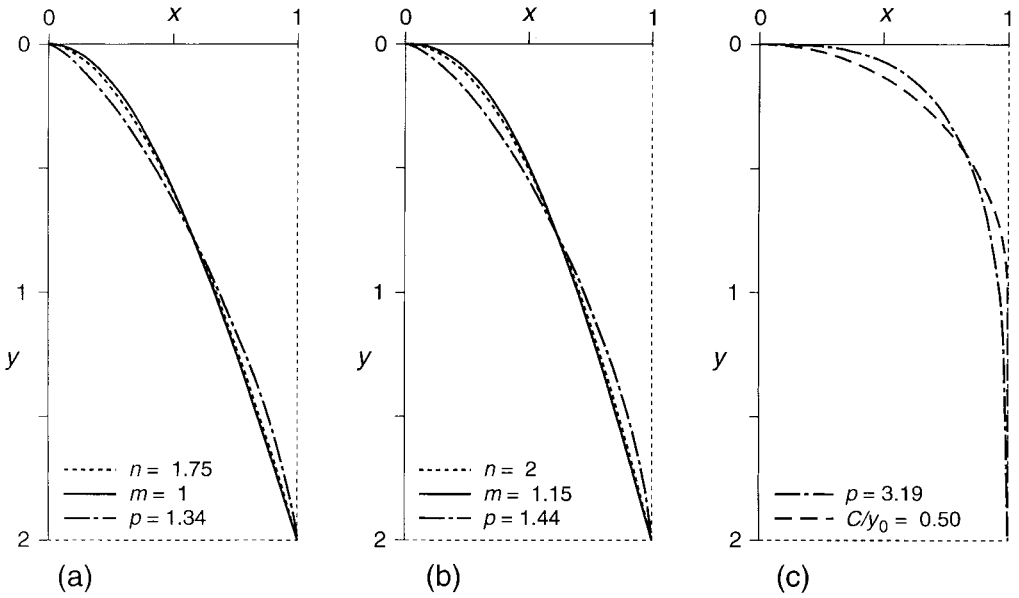

Fig. 6. Possible curves to fit the natural fold profiles represented by three points on the shape–amplitude diagram of Fig. 8: (a) point P, (b) point Q and (c) point R. All the curves have the same amplitude ($y_0/x_0 = 2$) and the normalised area is: (a) 1.27 (sine fit), (b) 1.33 (parabola fit) and (c) 1.78.

find the fitting function or functions whose area equals the area of the natural fold analysed. In the case of alloclinal folds, when Eq. (1) is used, the integration of this function allows us to determine the n value of the fitting function; this value is given by:

$$n = \frac{A}{x_0 y_0 - A}. \tag{6}$$

In the case of isoclinal folds, the fit by functions of the type (4) should be made by determining the parameter C, which can be derived from the formula of the area beneath the curve of Eqs. (4a) and (4b), and is given by

$$C = \frac{4A - \pi x_0 y_0}{x_0(4 - \pi)} \tag{7}$$

where x_0 and $y_0 = b + C$ can be measured on the natural fold (Fig. 3).

A graphical solution to obtain the value of the respective fold shape parameter, m or p, using Eq. (3) or Eq. (5), is shown in Fig. 5. In this figure all the fold shape parameters (n, C/y_0, m and p) have been included and mutually correlated through the area. In order to avoid the fold size effect in the determination of the parameters, a normalised area, defined as $\alpha = 2A/x_0 y_0$, and a normalised value of C (C/y_0) have been used in this figure. Hence, a fit by the area balance method permits the determination, from the normalised area below a natural fold profile, of the corresponding value of n, m, p and C/y_0, and therefore, of all the particular functions that can be used to describe the fold geometry.

The forms obtained from Eqs. (1), (3) and (5) for two particular cases of alloclinal folds, and from Eqs. (4a), (4b) and (5) for one particular case of isoclinal fold are shown in Fig. 6. Fig. 6(a) and (b) illustrate three profiles whose normalised area is that of the standard sinusoidal ($\alpha \approx 1.27$) and parabolic ($\alpha \approx 1.33$) shapes, respectively. Eq. (3) gives the perfect sinusoidal shape (Fig. 6a), whereas Eq. (1) gives the perfect parabolic shape (Fig. 6b). In both cases, Eqs. (1) and (3) exhibit forms very close, whereas Eq. (5) gives forms more separated from the standard shapes with tendency towards the pointed arch shape, and hence, less appropriate to fit the common alloclinal folds. Fig. 6(c) shows two profiles of isoclinal folds obtained from Eqs. (4a), (4b) and (5) for $\alpha \approx 1.79$; in this case, these functions represent two possible choices to fit isoclinal folds.

The accuracy of the fitting method by area balance results from the fact that the natural fold profile curve and the best-fit curve have the same y_0/x_0 value and the same concavity sense between the hinge point and the inflection point. Under these conditions, the deviation between both curves gives rise to two equal areas, one of them above the best-fit curve and another below it. When a natural fold profile is approximated by the best-fit function among Eqs. (1), (3), (4a), (4b) and (5), these areas are in general small, and the two curves are close. Inaccurate fits may result for some uncommon fold forms, but in these cases, the error is

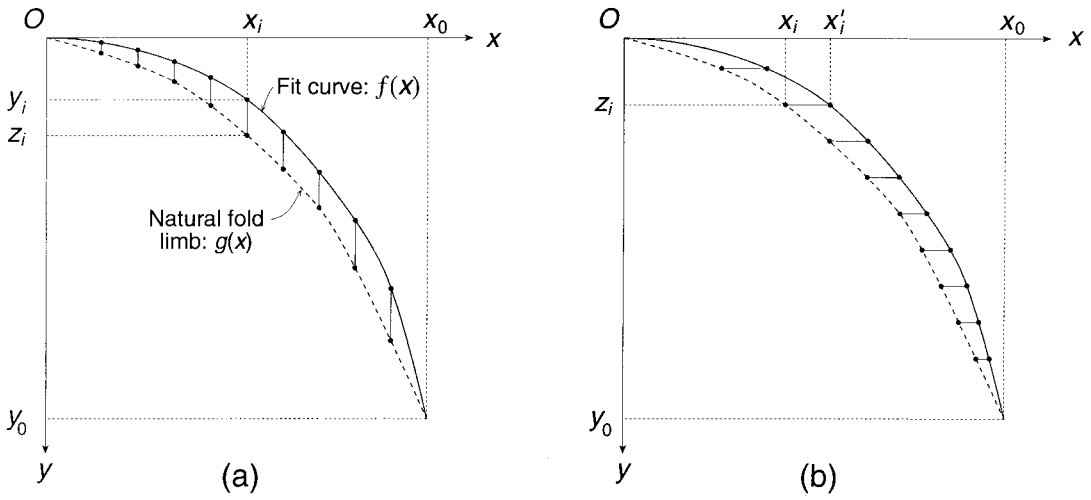

Fig. 7. Distances used to measure the fit error. (a) Along the y-axis. (b) Along the x-axis.

not due to the area-balance method, but to the inadequacy of the fitting functions.

3.2. Middle point fitting method

This method consists of finding a fitting function which passes through the point of the natural fold profile corresponding to $x = x_0/2$. For instance, introducing this condition for x in the power Eq. (1) and solving it for n, we obtain

$$n = \frac{\log y_0 - \log y_M}{\log 2} \tag{8}$$

where y_M is the value of Eq. (1) for $x = x_0/2$. The n value obtained enables us to define the fitting power function.

For isoclinal folds, in the case of Eqs. (4a) and (4b), the fitting function that passes through the point $(x_0/2, y_M)$ of the natural fold is defined by a C value given by:

$$C = y_0 - \frac{y_M}{1 - \frac{\sqrt{3}}{2}}. \tag{9}$$

The fitting method by coincidence of the functions using their x-middle point is easy to apply and offers a satisfactory approximation to the natural fold profiles.

3.3. Degree of misfit

The approximation of natural fold profiles to theoretical functions involves a degree of misfit that must be evaluated in order to know the accuracy of the fitting methods.

If $y_i = f(x_i)$ is the value of the fitting function [Eqs. (1), (3), (4a) and (4b) or Eq. (5)] for x_i, and $(x_1,z_1),(x_2,z_2),\ldots,(x_N,z_N)$ are points of the natural fold profile (Fig. 7a), the absolute rms error along the y-axis is given by

$$\varepsilon_y = \sqrt{\frac{1}{N}\sum_{i=1}^{N}(z_i - y_i)^2} \tag{10}$$

and the relative error expressed as a percentage is

$$\varepsilon_{y,r} = 100\frac{\varepsilon_y}{y_0}. \tag{11}$$

Similarly, if $z_i = g(x_i) = f(x_i')$ is the value of the function defined from the natural fold for x_i and of the fitting function for x_i' (Fig. 7b), the error along the x-axis is given by

$$\varepsilon_x = \sqrt{\frac{1}{N}\sum_{i=1}^{N}(x_i' - x_i)^2} \tag{12}$$

where $x_i' = f^{-1}(z_i)$. The corresponding relative error expressed as a percentage is

$$\varepsilon_{x,r} = 100\frac{\varepsilon_x}{x_0}. \tag{13}$$

From Eqs. (11) and (13), a total relative average error can be defined as

$$\bar{\varepsilon}_r = (\varepsilon_{x,r} + \varepsilon_{y,r})/2. \tag{14}$$

The fitting error affects several geometrical parameters of the analysed fold. In the case of alloclinal folds, one of these parameters is the maximum dip (Fig. 1a), which, in general, is different in the natural fold profile and the fitted curve. An absence of fitting error implies no error in the maximum dip; nevertheless, an absence of error in the maximum dip does not

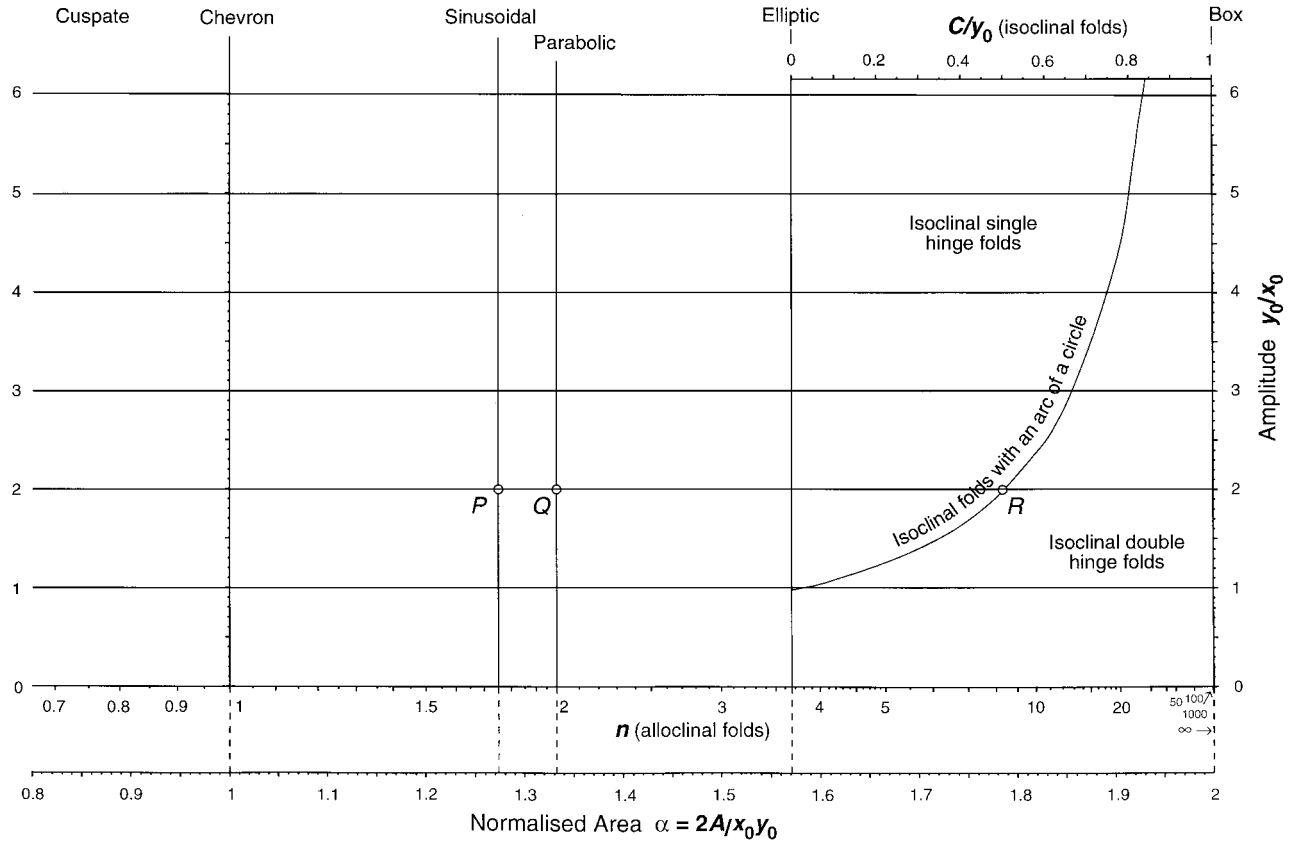

Fig. 8. Shape–amplitude classification diagram for folded surface profiles.

imply that there is no fitting error. It is not possible to determine exactly the fitting error by a single measurement; however, the error in the maximum dip is a good index of the fitting error which is very easy to obtain and also advantageous, since the maximum dip is a useful parameter in the geometrical description of folds. If β is the maximum dip measured on the fold profile and β^* is the maximum dip of the fitted curve, the relative error expressed as a percentage is given by

$$\varepsilon_A = 100(\beta^* - \beta)/\beta. \quad (15)$$

β can be directly measured from the drawing of the natural fold profile and β^* can be easily computed from the fitting power function [Eq. (1)]. In fact, $\tan\beta$ is given by

$$\tan\beta = (y')_{x_0} = y_0 n/x_0 \quad (16)$$

where $(y')_{x_0}$ is the derivative of Eq. (1) at $x = x_0$.

The determination of the fitting error permits determination of the best-fit function among the functions considered [Eqs. (1), (3), (4a), (4b) and (5)].

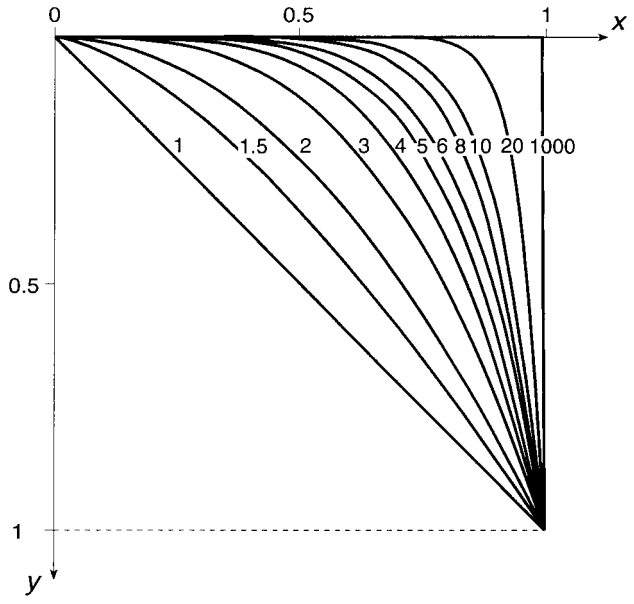

Fig. 9. Fold limb morphologies given by the power Eq. (1) for several n values (on the curves).

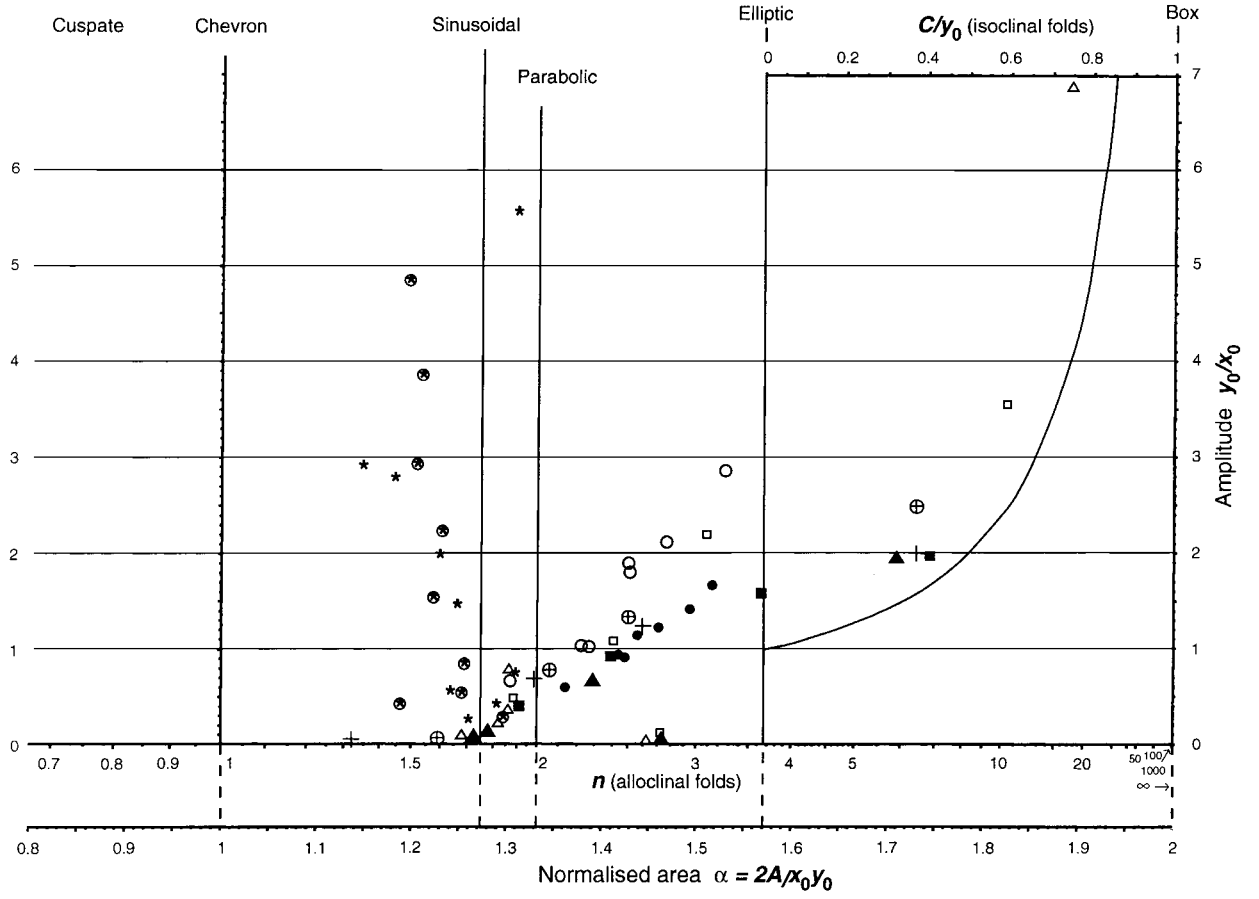

Fig. 10. Classification in the shape–amplitude diagram of fold profiles corresponding to several finite-element models of progressive folding in single layers. μ/μ_0 is the viscosity ratio between the folded layer and its host. Dieterich and Carter (1969, Fig. 2), $\mu/\mu_0=42.1$, ● outer arc, ○ inner arc. Hudleston and Stephansson (1973,Fig. 5B), $\mu/\mu_0=10$, ▲ outer arc, △ inner arc. *Ibid* (Fig. 8A), $\mu/\mu_0=100$, ■ outer arc, □ inner arc. *Ibid* (Fig. 8B), $\mu/\mu_0=1000$, + outer arc, ⊕ inner arc. Parrish et al. (1976, Fig. 9), equivalent $\mu/\mu_0=1$, ★ outer arc, ⊛ inner arc.

4. Classification of folded surface profiles

Fitting folded surface profiles with Eqs. (1), (3), (4a) and (4b) or Eq. (5) permits a simple and accurate graphical classification suitable for the analysis of fold sets (Fig. 8). The ratio y_0/x_0, which is a measurement of the fold amplitude (or an aspect ratio), will be the y-axis of the diagram. On the other hand, any of the shape parameters considered in Fig. 5 can be used as the x-axis. Nevertheless, the joint classification of alloclinal and isoclinal folds may require the combined use of two shape parameters. This is the reason why in the classification diagram of Fig. 8, the parameters n (alloclinal folds) and C/y_0 (isoclinal folds) have been chosen as the x-axis. Since the shape parameters are mutually related through the normalised area (α), this is a fundamental magnitude of the diagram, and it has also been incorporated in the x-axis on an arithmetic scale. This scale is appropriate to classify folded surfaces, because it weights very well the fold shape variation. Fig. 9 shows fold shapes for several n values; it appears that increasing n leads to changes in fold shape which are very different for low and high n values. For instance, an n change from 1 to 2 implies a variation in shape much greater than an n change from 20 to 21. Moreover, Fig. 9 shows that a close relationship occurs between changes in shape and changes in area. According to this, the arithmetic scale for α in the diagram in Fig. 8 represents adequately the change in fold shape.

Several fields have been separated in the classification diagram (Fig. 8) by lines that represent characteristic fold shapes (chevron, sinusoidal, parabolic, elliptic and box folds). A natural fold limb profile is represented in the diagram by a point. In the field where $n<3.66$, each point corresponds to an alloclinal fold with an n value that characterises the fold shape and an amplitude y_0/x_0. In the field where the scales for n and C/y_0 coexist, both isoclinal and alloclinal folds with $n\geq 3.66$ can be represented. Hence, each point corresponds to two folds with the same normalised area and amplitude y_0/x_0: an isoclinal fold characterised by a C/y_0 value, and an alloclinal fold characterised by a specific n value. Nevertheless, one

of these forms will fit the natural fold more closely. The form selected (isoclinal or alloclinal) must be indicated by a distinctive symbol. In general, this selection is straightforward, since each natural fold, alloclinal or isoclinal, will be better approximated by its respective function [Eq. (1) in the case of alloclinal folds or Eqs. (4a) and (4b) in the case of isoclinal folds]. If the selection is problematic, a method of error determination can be applied to choose the best fit.

In the isoclinal folds field, elliptical folds occur along the line $C/y_0 = 0$. The intersection point between $C/y_0 = 0$ and $y_0/x_0 = 1$ represents semi-circular folds. All the other isoclinal folds have a straight part and an elliptical part, and they can be plotted on the field for single hinge folds or on the field for double hinge folds. The folds plotted along the line that separates these fields include a circle arc. This line accomplishes the condition $x_0 = y_0 - C$, which implies that

$$\frac{C}{y_0} = 1 - \frac{x_0}{y_0}. \tag{17}$$

In Fig. 8, the shape parameters of Eqs. (1), (4a) and (4b) have been represented in the x-axis, but other parameters, such as those from Eqs. (3) and (5), can also be used on the diagram. Substituting the parameter represented along the x-axis does not involve changes in the location of the points plotted on the diagram, but it implies slight changes in the shape of the fold represented by each single point. Therefore, if the parameter represented on the x-axis is changed, the points P, Q and R of Fig. 8 can represent any of the respective shapes shown in Fig. 6.

5. Application of the fold classification method

To classify a limb profile of a folded surface on the shape–amplitude diagram (Fig. 8) we should follow these steps:

1. From a photograph, trace the fold profile onto transparent paper.
2. Locate the hinge and inflection points on the section and construct the reference frame.
3. Decide whether the fold is alloclinal or isoclinal and determine x_0 and y_0 on the drawing.
4. Use a fitting method to find the exponent n (alloclinal folds) or C/y_0 (isoclinal folds). If the area fitting method is chosen, the area beneath the curve (Fig. 1) must be measured; then, the n or C/y_0 value [or m or p values if Eq. (3) or Eq. (5) is chosen] can be obtained by plotting the area on the diagram in Fig. 5 or Fig. 8 as a normalised area ($\alpha = 2A/y_0x_0$), or by using Eq. (6) or Eq. (7) (only for n and C/y_0). If the middle point fitting method is chosen, the value y_M for $x = x_0/2$ must be measured and Eq. (8) or Eq. (9) must be used to obtain n or C.
5. Plot n (or m or p) and y_0/x_0 in the case of alloclinal folds, or C/y_0 (or p) and y_0/x_0 in the case of isoclinal folds on the diagram in Fig. 8 (or on its equivalent diagram for m or p). A different symbol must be used for points corresponding to alloclinal folds plotted within the isoclinal folds field, or in those cases in which two or more functions are used in a single diagram.

6. Examples

The capabilities of the classification method to characterise the geometry of folded surfaces are shown through its application to finite-element folds, experimental folds and natural folds.

6.1. Finite-element folds

Several folds obtained by finite element analysis have been represented in the classification diagram (Fig. 10) using the middle point fit method. These folds correspond to different sequences of progressive folding of a competent single layer embedded in an incompetent host. Most of the sequences were developed assuming Newtonian viscous models with an initial configuration corresponding to Biot's dominant wavelength and different viscosity contrasts (Dieterich and Carter, 1969, fig. 2; Hudleston and Stephansson, 1973, figs. 5B, 8A and B); the evolution of these models involves layer shortening, buckle shortening and flattening. Another model (Parrish et al., 1976, fig. 9) simulates the progressive folding of a quartzite layer embedded in marble, both with power constitutive flow law; in this model, buckling occurs until 20% of shortening is reached, and after that, flattening plays the dominant role.

The points corresponding to a single sequence describe approximate straight paths on the diagram. In the models with dominant buckle shortening, or with layer shortening and buckle shortening (Dieterich and Carter, 1969; Hudleston and Stephansson, 1973), an increase of n occurs when y_0/x_0 increases, so that an approximate linear relationship exists between the normalised area and y_0/x_0. In these models, the paths followed by the inner arcs exhibit a greater slope than the paths of the outer arcs. Moreover, the paths of the outer arcs are very close, suggesting that the shape evolution of these folded surfaces is independent of the viscosity contrast. More differences are observed between the paths of the inner arcs, for which an increase in the path slope seems to be related to a

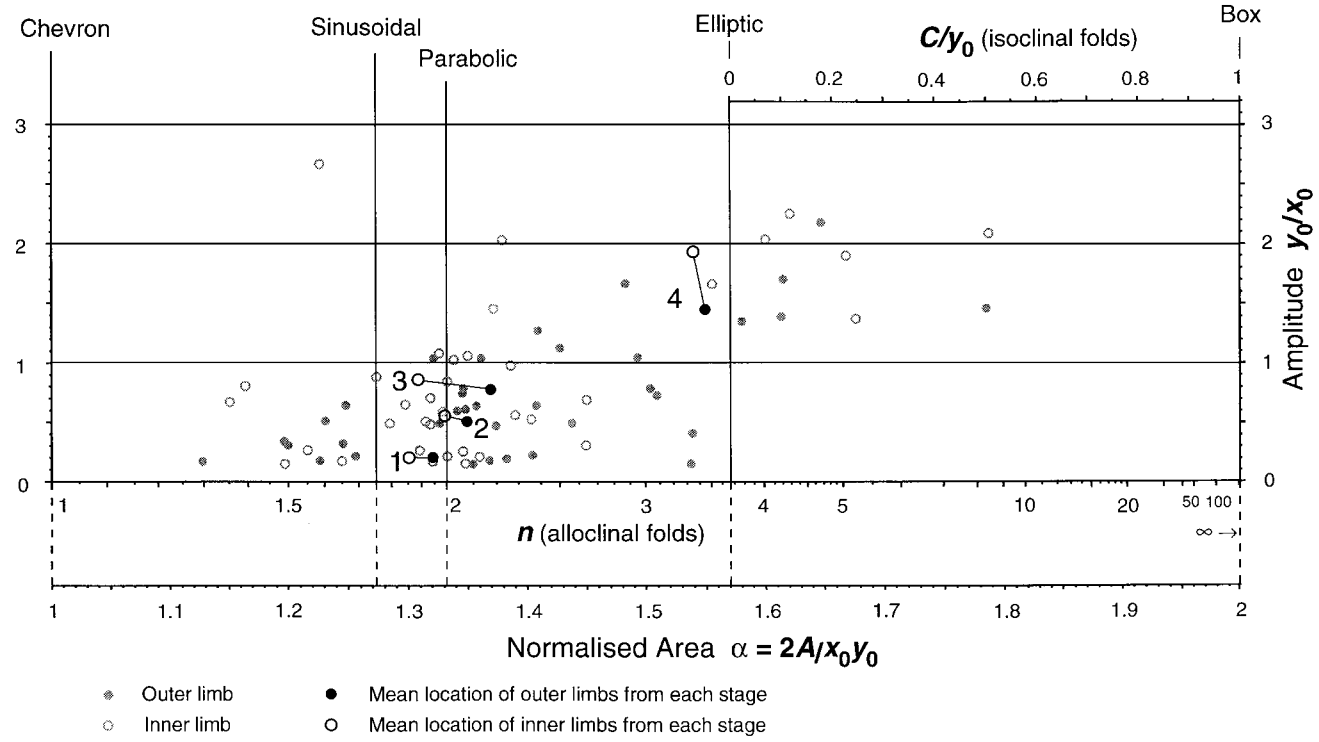

Fig. 11. Classification on the shape–amplitude diagram of the experimental buckling folds produced by Ramsay and Huber (1987, fig. 19.5) in a single layer of competent plasticine embedded in a matrix of soft plasticine.

decrease in the viscosity contrast. In the model where flattening superposed on previous buckling dominates, the paths are approximately vertical, so that y_0/x_0 increases keeping constant the n value.

6.2. Experimental folds

The folds classified have been taken from Ramsay and Huber (1987, fig. 19.5, folds E, F, G, f, and g, in stages 1–4) and correspond to a single layer buckling experiment (competent plasticine layer embedded in a less competent plasticine matrix). The classification results are shown in Fig. 11 and can be compared with those obtained by Ramsay and Huber (1987, fig. 19.24) using Hudleston's method. In spite of the high dispersion of points on the diagram, several features can be observed. The n-mean values for the first stage are located between the sinusoidal and parabolic folds, but as the amplitude increases, the folds progress toward more rounded shapes (sinusoidal → parabolic → elliptic → isoclinal). On the other hand, with the increase in amplitude, the mean value of the amplitude for the inner arcs increases in relation to that for the outer arcs.

6.3. Natural folds

Two examples of natural folds have been classified. The first one is a set of microscopic folds developed in a single layer of siltstone embedded in a much less competent slate matrix (from Ramsay and Huber, 1987, fig. 19.11). The second one is a multilayer of metasandstones and pelites (from Ramsay and Huber, 1987, fig. 15.15). The results of the classification are shown in Fig. 12.

In the case of the single layer, the points that represent inner arcs are separated from the points that represent outer arcs. Both sets of points exhibit increasing trends, with a higher slope for the inner arcs trend. On the other hand, in both sets the overturned limbs have higher values of n (or C/y_0) and y_0/x_0 than the normal limbs, as a result of the fold asymmetry.

In the multilayer, the points pattern is quite different. In the low amplitude folds, n values range from 1.5 to 2.5, whereas in the high amplitude folds, a trend toward the chevron shape is observed.

6.4. Comparison of results

The aim of this paper is not to gain insight into fold mechanics; nevertheless, the comparison of Figs. 10–12 is interesting in that respect. In all the single layer folds considered, except for those of Parrish et al. (1976) with equivalent $\mu/\mu_0 = 1$ (Fig. 10), an increase in amplitude involves an increase in n value with a nearly linear trend. In the finite-element and exper-

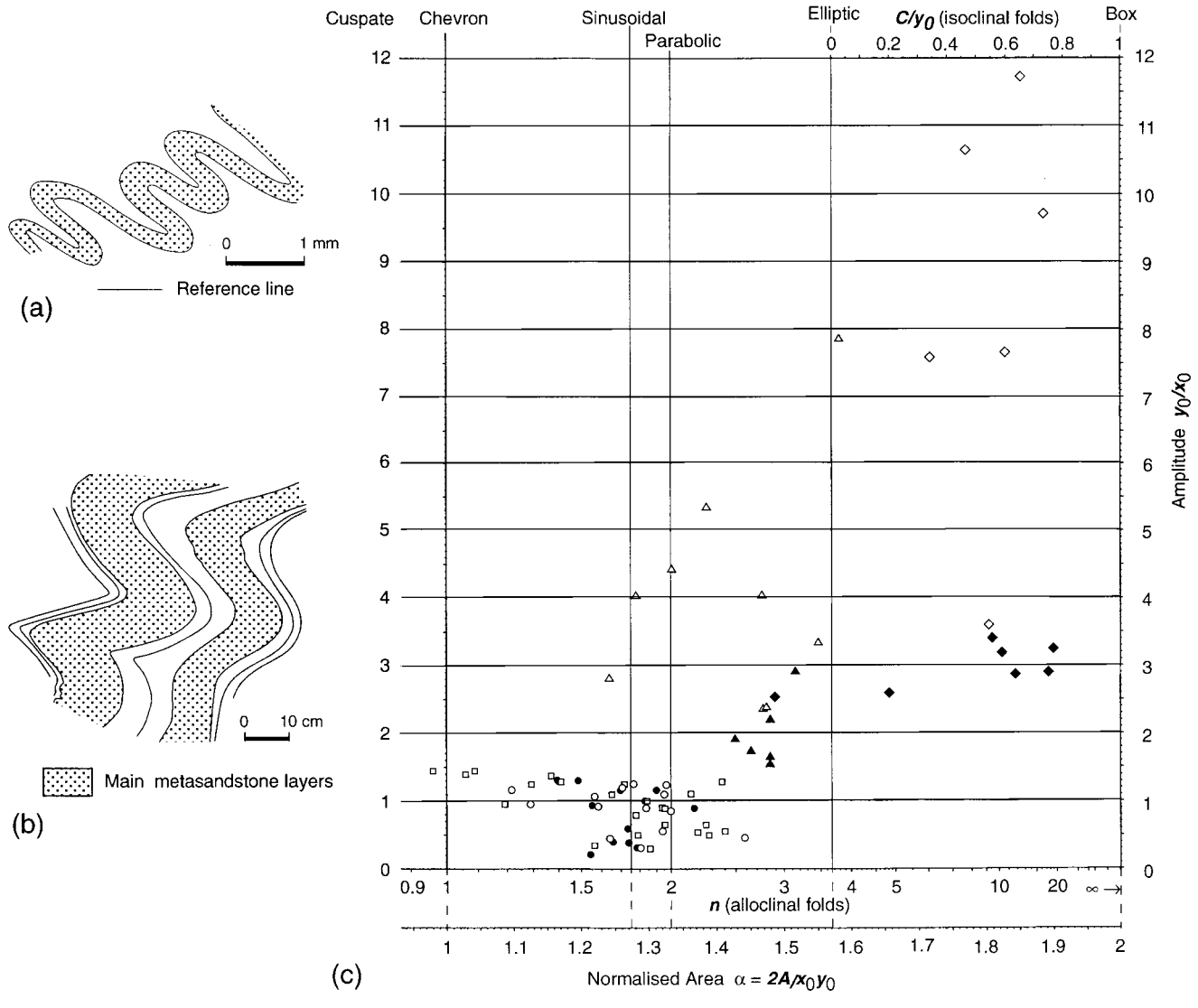

Fig. 12. Classification of the natural fold profiles shown in (a) and (b). (a) Microscopic siltstone layer embedded in slate (from fig. 19.11 of Ramsay and Huber, 1987); for the identification of normal and overturned limbs, the reference line is assumed to be horizontal. (b) Folds developed in a multilayer of metasandstones and pelites (from fig. 15.15 of Ramsay and Huber, 1987). (c) Classification in the shape–amplitude diagram.

imental folds, the trend reflects the fold geometry variation as fold amplifies, whereas in the natural folds, the trend results from the presence of folds with different evolution degrees in the photograph used. Nevertheless, it can be assumed that these evolution degrees are comparable to the progressive changes in shape of a single fold. Taking into account this assumption and that the materials simulated in the finite-element experiments of Dieterich and Carter (1969) and Hudleston and Stephansson (1973) have a linear rheological law, the similarity in shape of the experimental and natural folds (Figs. 11 and 12) suggests that these folds may have developed in layers with approximately linear rheology. The trend displayed by the multilayer folds toward the chevron shape (Fig. 12), suggests the participation of non-linear effects in the rock rheology, perhaps influenced by the layers mechanical interaction (cf. Johnson, 1970, pp. 297–298).

7. Discussion and conclusions

The present study is an attempt to provide a tool for the analytical systematisation of the folded surfaces geometry. To carry out this analysis folds have been

divided into alloclinal folds (interlimb angle > 0) and isoclinal folds (interlimb angle = 0).

The limb profiles of alloclinal folds are approximated by power functions [Eq. (1), Fig. 2] defined by three parameters (x_0, y_0 and n), which can be reduced to two (y_0/x_0 and n) if the fold size is not considered. y_0/x_0 characterises the fold amplitude and the exponent n characterises the fold shape. Therefore, depending on the value of n we have: $n<1$, cuspate folds; $n = 1$, chevron folds; $n = 2/(\pi - 2) \approx 1.75$, sinusoidal folds; $n = 2$, parabolic folds; $n \rightarrow \infty$, box folds. Eq. (3) is a more complicated choice to approximate alloclinal folds.

The limb profiles of isoclinal folds are approximated by functions [Eqs. (4a) and (4b), Fig. 3] which represent a quarter of an ellipse and a vertical segment of length C to describe the isoclinal part of the limb. In this case, y_0/x_0 also characterises the fold amplitude and the fold shape is defined by C/y_0, which varies from 0 (elliptic folds) to 1 (box folds).

Both alloclinal and isoclinal folds can be also approximated by superellipses (Gardner, 1965; Lisle, 1988) [Eq. (5)], although these functions are more complicated than Eqs. (1), (4a) and (4b) and in most cases give a worse approximation than Eq. (1) or Eq. (3) to the alloclinal natural folds. On the other hand, superellipses represent a complementary tool for the analysis of isoclinal folds.

This analytical description of the folded surfaces permits the construction of a shape vs amplitude (y_0/x_0) classification diagram (Fig. 8), in which both alloclinal and isoclinal folds can be plotted. The shape is represented on the x-axis by the parameters n (alloclinal folds) and C/y_0 (isoclinal folds) which overlap partially on this axis. Other parameters, such as m [Eq. (3)] or p [Eq. (5)] can be also used on the x-axis to describe the fold shape. All the parameters have been related by the area beneath the folded surface profile (Figs. 1 and 5), which has also been represented on the x-axis as a normalised area ($\alpha = 2A/x_0y_0$) (Fig. 8). Therefore, the proposed classification method permits approximation of a natural fold profile with several functions, so that one of them can be selected because of its fit quality or mathematical simplicity for the analysis of folding.

Unlike some previous classifications based on parameters which allow a graphical but not analytical description of folded surfaces (Fleuty, 1964; Ramsay, 1967; Twiss, 1988, amongst others), the classifications based on the approximation of folded surfaces by functions allow treatment of the folds as mathematical entities for their description and analysis. Obviously, the usefulness of a function depends on the degree of fit to natural forms and the simplicity of the function. In this respect, the functions used in this study permit the fitting of fold morphologies with a satisfactory precision using only two parameters, which in addition allows a graphical classification in a bidimensional diagram.

An attempt to fit fold geometry using a Fourier analysis with only two coefficients (b_1 and b_3) was carried out by Hudleston (1973). Nevertheless, this approximation does not adequately fit shapes such as chevron, elliptical or box folds (cf. fig. 15.12 of Ramsay and Huber, 1987). As a consequence, the analysis of Hudleston (1973) permits the labelling of fold surfaces with two parameters and their graphical classification, but it does not allow the use of the Fourier series for a functional description of folds. In addition, the standard amplitudes defined by Hudleston (1973) do not follow a regular pattern; for instance, according to the aspect ratio (y_0/x_0), amplitude 5 is twice amplitude 4, but amplitude 2 is 3.5 times amplitude 1. On the other hand, an approximation of fold morphologies using a greater number of Fourier coefficients provides more accuracy (Stowe, 1988), but does not permit either a simple graphical classification or an adequate functional description of folds, since the expressions involved are very complicated.

The method proposed in this paper permits the construction of visual charts to facilitate the classification of folded surfaces (Figs. 2 and 4). These charts can be easily adapted to the needs of any particular region. Nevertheless, we have not gained insight into this topic since the method proposed to determine the parameters involved in our classification (x_0, y_0, n and C) is simple and more accurate than visual methods.

The shape–amplitude diagram can be used in regional studies as a simple method to systematise accurately the geometry of large data sets of folded surfaces. In addition, this classification method permits comparison of the geometry of natural fold profiles with that of experimental and theoretical folds, as a tool to gain insight into the mechanics or mechanisms of folding. The representation of fold profiles by simple functions can be also useful in the theoretical analysis of the strain distribution in folded layers, since some of these functions can be easily introduced and transformed into the equations that describe the strain state of a rock.

Acknowledgements

Financial support from Spanish DGE 95-PB1047 and DGE 95-PB1052 projects is acknowledged. We are grateful to Richard J. Lisle, Josep Poblet, Heather Stoll and Robert J. Twiss for many valuable suggestions. Richard J. Lisle drew our attention to the superellipses previously used by him to analyse clastic particles.

References

Bastida, F., 1993. A new method for the geometrical classification of large data sets of folds. Journal of Structural Geology 15, 69–78.

Cooper, M.A., Garton, M.R., Hossack, J.R., 1983. The origin of the Basse Normandie duplex, Boulonnais, France. Journal of Structural Geology 5, 39–52.

Dieterich, J.M., Carter, N.L., 1969. Stress-history of folding. American Journal of Science 267, 129–154.

Fleuty, M.J., 1964. The description of folds. Proceedings of the Geological Association of London 75, 461–492.

Gardner, M., 1965. The ''superelipse'': a curve that lies between the elipse and the rectangle. Scientific American 213, 222.

Hudleston, P.J., 1973. Fold morphology and some geometrical implications of theories of fold development. Tectonophysics 16, 1–46.

Hudleston, P.J., Stephansson, O., 1973. Layer shortening and fold shape development in the buckling of single layers. Tectonophysics 17, 299–321.

Johnson, A.M., 1970. Physical Processes in Geology. Freeman, San Francisco.

Lisle, R.J., 1988. The superellipsoidal form of coarse clastic sediment particles. Mathematical Geology 20, 879–890.

Lisle, R.J., 1997. A fold classification scheme based on a polar plot of inverse layer thickness. In: Sengupta, S. (Ed.), Evolution of Geological Structures in Micro- to Macro-scales. Chapman & Hall, London, pp. 323–339.

Parrish, D.K., Krivz, A.L., Carter, N.L., 1976. Finite-element folds of similar geometry. Tectonophysics 32, 183–207.

Ramsay, J.G., 1967. Folding and Fracturing of Rocks. McGraw-Hill, New York.

Ramsay, J.G., Huber, M.I., 1987. Modern Structural Geology, Volume 2: Folds and Fractures. Academic Press, London.

Stabler, C.L., 1968. Simplified Fourier analysis of fold shapes. Tectonophysics 6, 343–350.

Stowe, C.W., 1988. Application of Fourier analysis for computer representation of fold profiles. Tectonophysics 156, 303–311.

Twiss, R.J., 1988. Description and classification of folds in single surfaces. Journal of Structural Geology 10, 607–626.